Thermal stability of Mg2Si0.55Sn0.45 for thermoelectric applications

Mahdi Mejri, Benoît Malard, Yohann Thimont, Krunoslav Romanjek, Hilaire Ihou Mouko, Claude Estournès

Thermal stability of $Mg_2Si_{0.55}Sn_{0.45}$ for thermoelectric applications

M. Mejri [a], B. Malard [b], Y. Thimont [a], K. Romanjek [c], H. Ihou Mouko [d], C. Estournès [a, *]

[a] CIRIMAT, Université de Toulouse, CNRS, Université Toulouse 3 - Paul Sabatier, 118 Route de Narbonne, 31062, Toulouse cedex 9, France
[b] CIRIMAT, Université de Toulouse, CNRS, Toulouse INP, 4 allée Emile Monso, 31030, Toulouse cedex 4, France
[c] CEA-LITEN, Université Grenoble Alpes, 17 rue de martyrs, F-38000, Grenoble, France
[d] HotBlock OnBoard, 43 chemin du vieux chêne, F-38240, Meylan, France

ARTICLE INFO

Keywords:
Thermoelectric materials
Silicide $Mg_2(Si,Sn)$
Pesting
Thermal stability
Phase separation
Kirkendall effect
Porosity

ABSTRACT

Understanding the thermal stability of the $Mg_2(Si,Sn)$ system is essential to define their safe temperatures of service. Despite its good thermoelectric performance, $Mg_2(Si,Sn)$ is subject to a phase separation during thermal cycling due to the miscibility gap, which leads to a degradation of its thermoelectric properties and affects its performance during device operation. Isothermal annealing at 500 °C and 750 °C were performed with different annealing time to investigate thermal stability of $Mg_2(Si,Sn)$. During the heat treatment, two phases were formed associated with porosity in the matrix. In addition, thickness of specimen was tracked and a significant expansion was detected. This phenomenon is attributed to the Kirkendall effect. The composition and the structure of the two forming phases were investigated by electron probe microanalysis and X-ray diffraction. Finally, the optimized thermal treatment allowed to stabilize the $Mg_2(Si,Sn)$ without porosity and the presence of two thermodynamically stabilized phase ($Mg_2Si_{0.41}Sn_{0.59}$ and $Mg_2Si_{0.58}Sn_{0.42}$) leading to a better reliability of the silicide thermoelectric modules.

1. Introduction

For several years, researchers are focusing on the energy efficient devices to enhance power production due to the high increase of its consumption around the world. To accomplish such goals scientists are massively attracted towards thermal energy conversions to generate electricity. To increase the diversity of the energetic choices the appropriate material selection significantly aids in the development of efficient thermoelectric (TE) devices. In the current era, many researchers are working on the production of thermoelectric generators (TEG). Significant progress has been observed in the discovery of materials with important factor of merit ZT [1–4].

In the last four decades, for medium temperature applications, silicides were identified due to their good thermoelectric performances, high abundance, low-cost and more they are eco-friendly materials. They have relatively high ZT (~1.1–1.5) compared to those found on the market for applications at the same temperature range [5–8]. However, in contrast to bismuth telluride [1], their industrial development still require more effort to improve their chemical, thermal and mechanical stability, synthesis methods, shaping and production costs. Thermal stability of the selected legs is one of the key issues in thermoelectric applications [1,9]. $Mg_2(Si,Sn)$ is not stable and may be subjected to phase separation during long-term applications [10,11] or cycling [12,13]. However, very few studies have been devoted to the thermal stability of $Mg_2(Si,Sn)$ [13–18].

The evaluation of the pseudo-binary $Mg_2(Si,Sn)$ system has been a subject of several investigations. The literature provides at least four different versions of the $Mg_2(Si,Sn)$ pseudo-binary diagram obtained experimentally [5,19–21] and by thermodynamic modelling [13,22–24]. The main differences between these phase diagrams concern miscibility gap width of the $Mg_2(Si,Sn)$ solid solution. For example, the first investigation of the Mg_2Si–Mg_2Sn binary diagram was carried out by Muntyanu et al., in 1966 [19] which propose a phase diagram showing two solid solutions $Mg_2Si_{0.4}Sn_{0.6}$ (Sn-rich) and $Mg_2Si_{0.9}Sn_{0.1}$(Si-rich) with a peritectic equilibrium at 860 °C. In 1968, Nikitin et al. [20] investigated the same phase diagram ($Mg_2(Si,Sn)$) and reported a phases diagram with two solid solutions $Mg_2Si_{0.4}Sn_{0.6}$ (Sn-rich) and $Mg_2Si_{0.6}Sn_{0.4}$ (Si-rich) with a peritectic equilibrium at 860 °C. According to the latter publication [20], this difference is explained by longer annealing times and slower crystallization which allows to reach

* Corresponding author.
E-mail address: estournes@chimie.ups-tlse.fr (C. Estournès).

https://doi.org/10.1016/j.jallcom.2020.156413

the thermodynamic equilibrium.

Therefore, thermal stability of these materials must be ensured as a function of time and temperature. In the present article, annealing tests were carried out at different temperatures and times in order to reach thermodynamic equilibrium and to stabilize the present phases in the compound of composition: $Mg_2Si_{0.55}Sn_{0.45}$. The effect of time and temperature annealing was studied by performing dilatometry analysis followed by characterization of the microstructure of the annealed samples using scanning electron microscope (SEM) and electron probe microanalyser (EPMA) techniques.

2. Experimental procedure

Pellets prepared with expected $Mg_2Si_{0.55}Sn_{0.45}$ composition were synthesized using commercial high purity powders of Mg (99%), Si (99.9%) and Sn (99.9%). Powder was sintered in a graphite die of Ø 60 mm through the spark plasma sintering (SPS) at 750 °C under 50 MPa by the industrial partner HotBlock OnBoard (HBOB). To investigate the stability of the sample and to achieve thermodynamic equilibrium (referred to pseudo binary diagram of Mg_2Si–Mg_2Sn), several heat treatments have been carried out on the sintered material. Parts of the pellets were cut with a thickness of 4 mm then have been annealed and thermally analyzed in a dilatometer (Setaram Setsys Evo with heating and cooling rate of 5 °C/min) under argon gas protection for 20, 40, 60 and 80 h up to 500 °C. Moreover, samples were annealed at 750 °C for 0.5, 1, 2 and 3 h under argon gas protection.

The sintered and annealed samples were investigated by SEM (VEGA3 Tescan) and energy dispersive X-ray spectroscopy (EDX) and electron probe microanalysis (EPMA). X-ray diffraction (XRD) patterns were taken on some annealed samples (500 °C) utilizing a Bruker D8-advanced diffractometer with Cu Kα radiation (1.5406 Å) in the 2θ range 20–70° with a step size of 0.01°.

High-energy X-ray diffraction (HEXRD) experiments were performed on powder, sintered and annealed (750 °C) material on the P07 beamline at the Deutsches Elektronen Synchrotron (DESY, Hamburg, Germany). The measurements were conducted with a 103 keV (0.119987 Å) monochromatic beam (5 × 300 μm^2 size) which allowed us to analyze in transmission the large volume of the sample (due to the low absorption of the elements consisting the sample) so lessening the surface effect. The transmitted signal was collected by a large-area 2D detector (PerkinElmer XRD1621) that recorded the whole Debye–Scherrer rings with a maximum 2θ angle of 12°.

3. Results and discussion

3.1. Thermoelectric generator failure

Fig. 1a presents a TEG manufactured by the industrial Partner HBOB with two legs of high manganese silicide (HMS) and two legs of $Mg_2Si_{0.55}Sn_{0.45}$ [8]. The generator was obtained by soldering the thermoelectric legs with metallized ceramics plates (AlN-DBC) using a silver solder. The diffusion barrier between the (n & p)-type and the solder consists of a thin layer of Au/Ti (300/100 nm). This TEG was tested on a dedicated bench [25] in CEA laboratory (Grenoble-France) with a large number of thermal cycles applied on the hot side of TEG between 150 and 400 °C, with 3 min of holding at 400 °C for a total duration of 15 min per cycle. The cold side is maintained at 50 °C during thermal test. After 100 h (400 cycles) of testing, the TEG became out of order due to fractures (cracks) localized in the hot side of the n-type legs (Fig. 1b). During thermal test, we noticed an increase of the internal electric resistance of the TEG probably due to the formation of a thin layer of MgO (revealed with SEM/EDS analysis) and a diffusion layer between the $Mg_2(Si,Sn)$ (n-type) and the solder (Ag) in the hot side of the legs. Moreover, some cracks located near the TM-solder hot interface appeared which can also increase the internal electric resistance of TEG. Similar results are reported by Skomedal et al. [12] showing the appearance of cracks and diffusion layer (MgO) in the hot side of the leg.

This mechanical disintegration of the n-type at 400 °C could be related to a pesting phenomenon [26–28]. According to Fitzer et al. [27], pesting effect occurring to the material is caused by internal stress enhanced oxidation. The accommodation of residual stress coupled with oxidation lead eventually to brittle fracture so no electric generation. The pesting is only present in the hot side of $Mg_2(Si,Sn)$ legs. The cold side being intact on its side. Oxidation and decomposition of $Mg_2(Si,Sn)$ have been shown to be a critical problem when tests are performed in an oxygen atmosphere at a partial pressure of at least 0.9 bar. Clearly, the Au/Ti diffusion barrier has not stopped Mg or Sn to diffuse to the interface between $Mg_2(Si,Sn)$ and Ag and react with oxygen.

3.2. Structural and microstructural properties of $Mg_2(Si,Sn)$ before and after sintering

The XRD spectrum of $Mg_2Si_{0.55}Sn_{0.45}$, before and after sintering, are presented in Fig. 2. Pattern analysis of $Mg_2Si_{0.55}Sn_{0.45}$ powder has revealed the presence a different solid solution $Mg_2Si_{1-x}Sn_x$ with different phases such as Mg_2Si (JCPDS file n°00-035-0773), Mg_2Sn (JCPDS file n° 00-007-0274), Si (JCPDS file n° 000-065-2871) and Sn (JCPDS file n°03-065-0297). After sintering, no residual Mg, Si, Sn, Mg_2Si and Mg_2Sn phases were found and all peaks apparently match well with a single phase corresponding to an eventual $Mg_2Si_{0.55}Sn_{0.45}$ phase. Nevertheless, XRD pattern of the compound after sintering presents clearly asymmetric peaks. This asymmetry means that the material has a composition gradient which induce small lattice parameters differences. This composition gradient is due to the powders manufacturing and to the short sintering time (5 min) which is insufficient to ensure the full reaction of all the grains with each other. We can also notice the width of the peak which decreases with the sintering in agreement with a grain growth due to the sintering process.

Fig. 3 shows a SEM micrograph of the typical microstructure of the 750 °C-sintered $Mg_2Si_{0.55}Sn_{0.45}$ through the SPS process. SEM micrograph of this compound confirms clearly the presence of several phases with domains with various contrasts. The brighter phase is the richest in Sn while the dark phase is enriched in Si. A high relative density of 99% was confirmed by the Archimedes method. Residual porosity (identified by dark areas) exists even after sintering process. Consequently, it can be concluded that after SPS process at 750 °C for 5 min, $Mg_2Si_{0.55}Sn_{0.45}$ compound is heterogeneous with the presence of very few residual porosity, which could be a sign of instability and limits the reliability of the legs.

3.3. Structural and microstructural properties of $Mg_2Si_{0.55}Sn_{0.45}$ after annealing at 500 °C

The XRD patterns of $Mg_2Si_{0.55}Sn_{0.45}$ compound after 20, 40, 60 and 80 h of annealing at 500 °C in a dilatometer are presented in Fig. 4. The samples after dilatometry analysis were examined by SEM and some transformation areas were observed. Fig. 5 shows the microstructure of the sample after 60 h of heat treatment. It is composed of a dark-phase distributed in a bright more or less percolating phase (matrix). The observed contrast suggests that the dark domains are Si rich and the bright domains are Sn rich. This seems to be in agreement with some studies which reported that $Mg_2Si_{1-x}Sn_x$ solid solutions decompose into two phases (Sn-rich

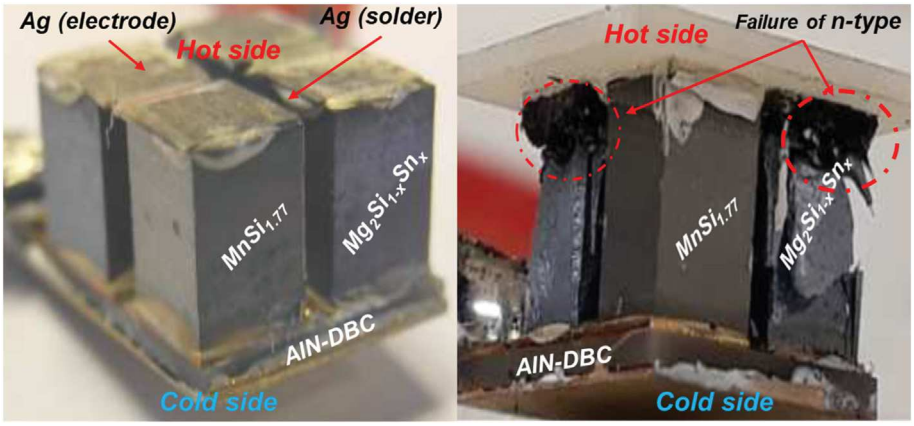

a) b)

Fig. 1. a) Thermoelectric generator before thermal test and b) after cycling thermal test for 100 h (150–400 °C).

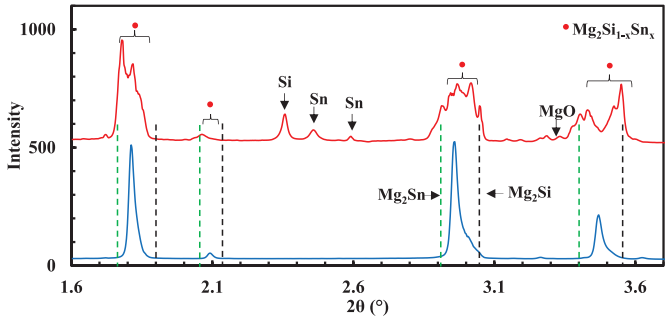

Fig. 2. XRD patterns for $Mg_2Si_{0.55}Sn_{0.45}$ powder (red) and after sintering (blue) at 750 °C for 5 min. (For interpretation of the references to colour in this figure legend, the reader is referred to the Web version of this article.)

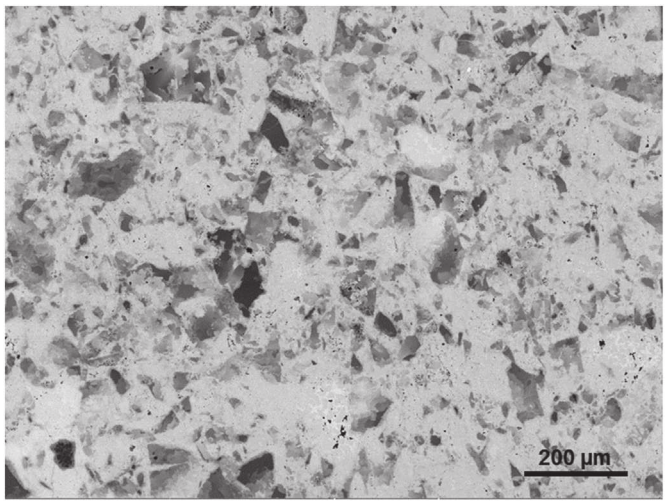

Fig. 3. SEM micrographic (BSE) of $Mg_2Si_{0.55}Sn_{0.45}$ after sintering for 5 min at 750 °C. The brighter phases are Sn enriched and the dark phases are Si enriched. Polishing was carried out in ethanol to avoid oxidation.

and Si-rich) due to a peritectic reaction [13].

Fig. 6 represent the displacement versus temperature of the sintered (not annealed) sample for 20, 40 and 60 h of annealing at 500 °C under argon gas protection. During annealing, a significant expansion of the sample was detected (~30 µm after 60 h). The thickness increase of the sample is however related to the expansion of the material volume caused by the significant porosity forming in the Sn-rich matrix due to the Sn migration and the separation of the two phases (Sn-rich and Si-rich) which have two different lattice parameters. The difference between the diffusion coefficients of Sn and Si generate a lacuna flux, which provide voids located in the Sn-rich (matrix). This effect is known as the Kirkendall effect [29] and lead to the presence of porosity which can reduce the mechanical properties of the material [8].

This phenomenon is schematized in Fig. 7 in the case of our compound leading to a phase separation and volume expansion due to the presence of porosity. After sintering, the $Mg_2(Si,Sn)$ is unstable and exhibits gradient composition and low level of porosity. During annealing, Sn diffuses to the Mg_2Si, which enhances the Si-rich and Sn-rich phase formation phases and generates porosities in the matrix (Sn-rich). The Kirkendall effect occurs at the boundary junction of two metals as a result of differences in the diffusion rates of different metal atoms which it is difficult to balance a fast-diffusion with a slow one [29]. As result, a volume expansion is due to the increasing of porosity in the material. A shift of the peaks to lower angles is observed, with annealing time, on these patterns which can indicate a phase evolution of the sample during the thermal annealing and/or an increase in tensile stress in the phase concerned [30,31].

3.4. Annealing process for stabilization of the compound

The XRD patterns of sample, after 0.5, 1 and 2 h of annealing at 750 °C are presented in Fig. 8. A shift of the peaks to lower angles is observed, with annealing time, on these patterns which can indicate a phase evolution of the sample during the thermal annealing. However, the resolution of XRD patterns is not sufficient to unambiguously identify the nature of the phases, this point will be discussed below using HEXRD patterns.

Fig. 9 shows the SEM micrography of the $Mg_2Si_{0.55}Sn_{0.45}$ compound after heat treatment for 3 h at 750 °C. As for the samples treated at 500 °C the separation of the two phases, Sn-rich and Si-rich which have two different lattice parameters, is evidenced. The chemical composition of the two phases given in Table 1, investigated by EPMA, are average values of at least 30 measurements. Both composition are in agreement with the determination of the stoichiometry compound given in Nikitin et al. [20]. According to Zaitsev et al. [5], the two solid solutions, Sn-rich ($Mg_2Si_{0.4}Sn_{0.6}$) and Si-rich ($Mg_2Si_{0.6}Sn_{0.4}$), both had good thermoelectric properties.

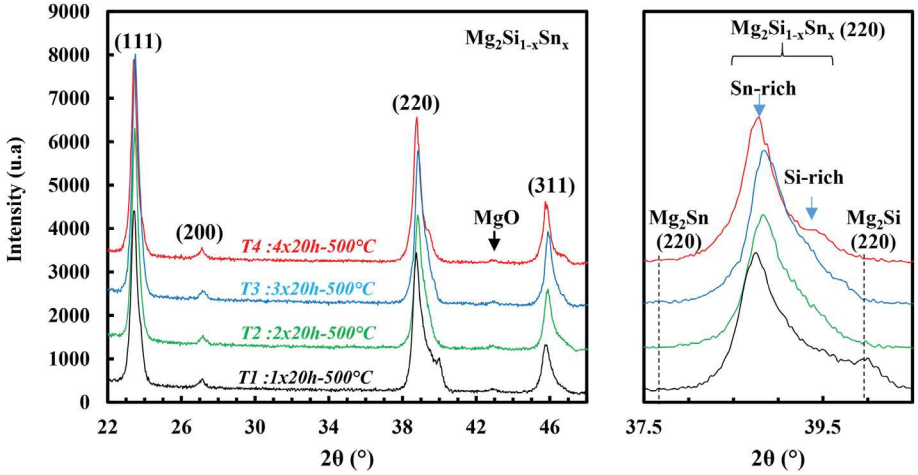

Fig. 4. XRD patterns of $Mg_2Si_{0.55}Sn_{0.45}$, which was made by SPS and annealed for 20, 40, 60 and 80 h at 500 °C.

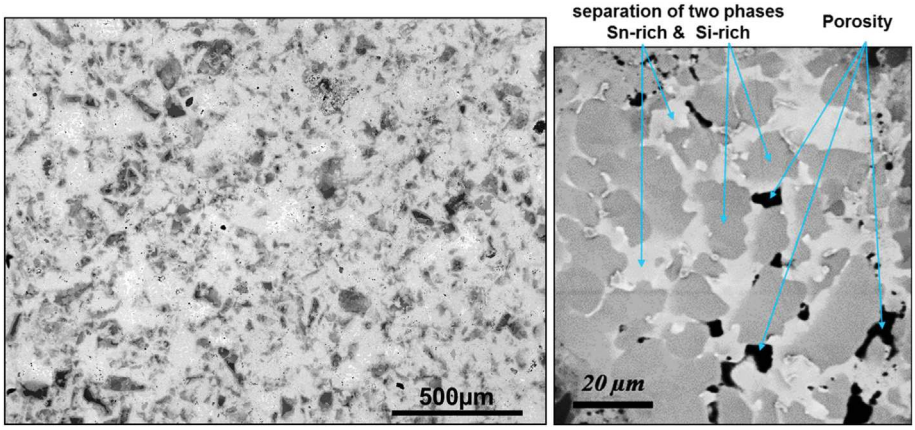

Fig. 5. (Left) SEM micrographic (BSE) of $Mg_2Si_{0.55}Sn_{0.45}$ after heat treatment for 60 h at 500 °C. Si-rich (grey), Sn-rich, porosity (black), Sn (white). (Right) Zoom of one of observed transformation area.

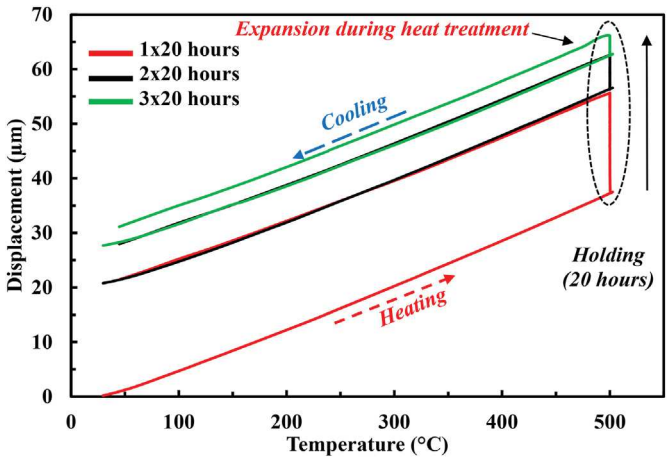

Fig. 6. Displacement versus temperature of $Mg_2Si_{0.55}Sn_{0.45}$ after 20 h (red), 40 h (black) and 60 h (green) under Argon gas protection. (For interpretation of the references to colour in this figure legend, the reader is referred to the Web version of this article.)

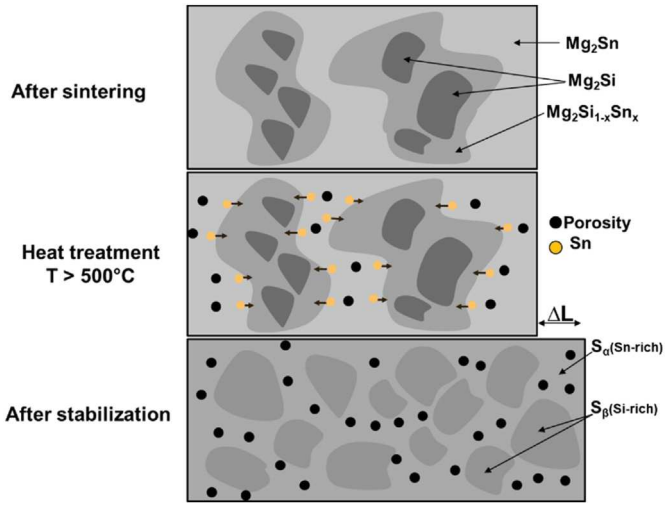

Fig. 7. Scheme of formation of the Kirkendall effect in $Mg_2(Si,Sn)$ phases separation.

Nevertheless, it still necessary to check the presence of the two phases using high resolution XRD pattern.

Fig. 10 shows the HEXRD pattern (100 × 300 × 3000 µm^3-gauge volume) acquired on the $Mg_2Si_{0.55}Sn_{0.45}$ compound annealed at 750 °C for 3 h under argon gas protection. This HEXRD pattern

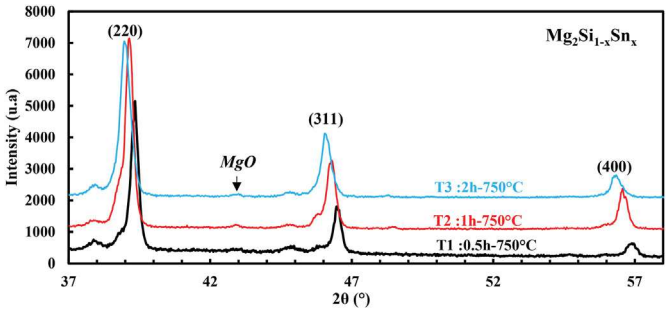

Fig. 8. XRD patterns of $Mg_2Si_{0.55}Sn_{0.45}$, which was made by SPS and annealed for 0.5, 1 and 2 h at 750 °C.

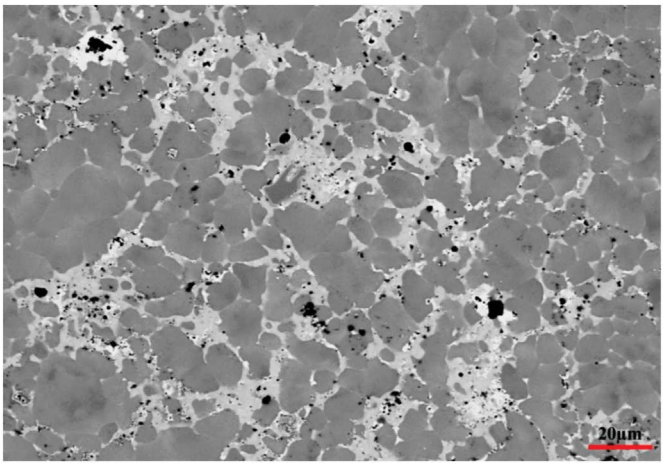

Fig. 9. SEM micrographic (BSE) of $Mg_2Si_{0.55}Sn_{0.45}$ after heat treatment for 3 h at 750 °C (Si-rich (grey), Sn-rich, porosity (black), Sn (white).

Table 1
Chemical compositions corresponding to the two phases Si-rich and Sn-rich according to the literature and the results of our work.

References	S_α (Sn-rich)	S_β (Si-rich)
Muntyanu [17]	$Mg_2Si_{0.38}Sn_{0.62}$	$Mg_2Si_{0.83}Sn_{0.17}$
Nikitin [18]	$Mg_2Si_{0.38}Sn_{0.62}$	$Mg_2Si_{0.59}Sn_{0.41}$
Kozlov [21]	$Mg_2Si_{0.06}Sn_{0.94}$	$Mg_2Si_{0.74}Sn_{0.26}$
This work	$Mg_2Si_{0.41}Sn_{0.59}$	$Mg_2Si_{0.58}Sn_{0.42}$

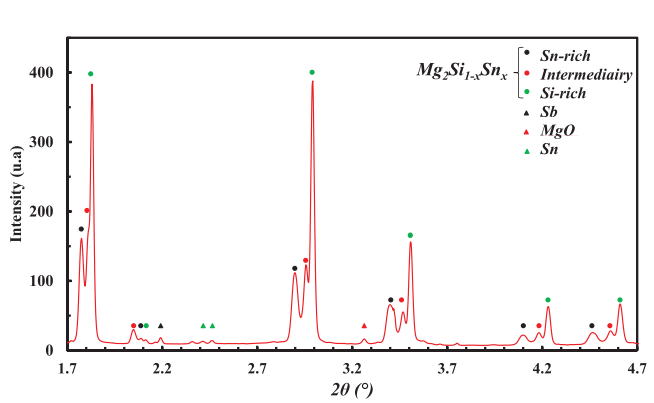

Fig. 10. HEXRD pattern of $Mg_2Si_{0.55}Sn_{0.45}$ after annealing for 3 h at 750 °C (100 × 300 × 3000 μm^3-gauge volume).

Table 2
Chemical compositions and calculated lattice parameter corresponding to the two phases Si-rich and Sn-rich.

Phases	Composition	a (Å)	Rwp
Sn-rich	$Mg_2Si_{0.41}Sn_{0.59}$	6.7073(3)	6.3
Intermediary	$Mg_2Si_{1-x}Sn_x$	6.5766(4)	7.1
Si-rich	$Mg_2Si_{0.58}Sn_{0.42}$	6.4979(9)	8.1

confirms clearly the presence of the two phases (in agreement with the presence of the miscibility gap). Rietveld refinement [32] was performed on XRD data of the annealed sample with FullProf software [33]. The calculated lattice of forming phases are listed in Table 2. The Si-rich phase is $Mg_2Si_{0.58}Sn_{0.42}$ with a lattice parameter of 6.4979 Å while the Sn-rich phase is $Mg_2Si_{0.41}Sn_{0.59}$ with a lattice parameter of 6.7073 Å. These results are in coherence with the thermodynamically steady state phase diagram given by Nikitin et al. [20].

After heat treatment, the sample was tested in the dilatometer up to 500 °C for 2 h of holding (Fig. 11) and no more expansion was detected at this stage. Here, we can consider that the thermal stability of $Mg_2Si_{0.55}Sn_{0.45}$ was then reached after 3 h at 750 °C of annealing. Even though the thermoelectric properties of the stabilized material have not yet been measured, Zaitsev et al. [5] reported that both solid solutions Si-rich and Sn-rich ($x = 0.4$ and $x = 0.6$), have the best ZT at high temperatures, one can expect that the TE properties of the compound will not be degraded but possibly increased once it is stabilized. The work presented here aims to stabilize of the $Mg_2Si_{0.55}Sn_{0.45}$ compound and to characterize its structure and its microstructure after several heat treatment conditions. Further work is warranted in order to get the thermoelectric properties of the stabilized material and the evaluation of its performance in TEG modules.

4. Conclusion

$Mg_2(Si,Sn)$ is promising thermoelectric material due to its well-known good thermoelectric performances and non-toxicity. However, it is subjected to degradation, under thermal cycling, as a result of phase separation caused by the miscibility gap in the binary Mg_2Si–Mg_2Sn system. In this study, thermal stability of $Mg_2Si_{0.55}Sn_{0.45}$ compound was investigated. The effect of time and temperature annealing was studied by performing dilatometry analysis followed by characterization of the microstructure of the annealed samples.

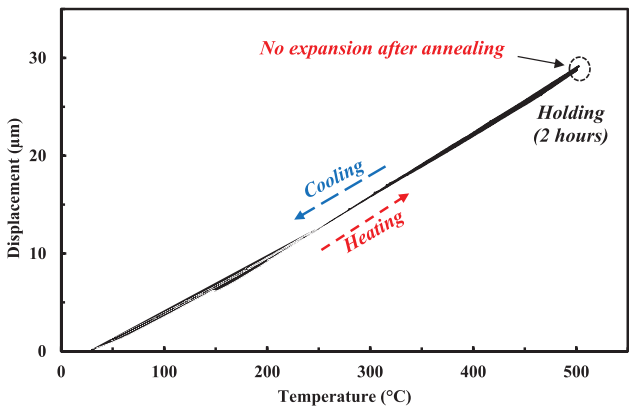

Fig. 11. Displacement versus temperature of $Mg_2Si_{0.55}Sn_{0.45}$ compound after annealing for 3 h at 750 °C.

XRD, HEXRD and SEM results show that, after annealing for 3 h at 750 °C, $Mg_2(Si,Sn)$ presents two phases with different compositions and lattices parameters. During annealing, $Mg_2Si_{0.55}Sn_{0.45}$ segregates into two phases Si-rich ($Mg_2Si_{0.58}Sn_{0.42}$, a = 6.4979 Å) and Sn-rich ($Mg_2Si_{0.41}Sn_{0.59}$, a = 6.7073 Å) creating porosity in the matrix which was explained by the Kirkendall effect. In summary, the thermal stability of $Mg_2Si_{0.55}Sn_{0.45}$ was achieved after 3 h of annealing at 750 °C. It should increase the reliability of $Mg_2Si_{0.55}Sn_{0.45}$ legs at high temperature operating conditions for silicides TEG modules.

CRediT authorship contribution statement

M. Mejri: Methodology, Investigation, Validation, Writing - original draft. **B. Malard:** Methodology, Investigation, Validation, Writing - review & editing. **Y. Thimont:** Methodology, Investigation, Validation, Writing - review & editing. **K. Romanjek:** Conceptualization, Writing - review & editing. **H. Ihou Mouko:** Conceptualization, Provision of study materials, Writing - review & editing. **C. Estournès:** Conceptualization, Methodology, Investigation, Validation, Writing - review & editing, Supervision, Project administration.

Declaration of competing interest

The authors declare that they have no known competing financial interests or personal relationships that could have appeared to influence the work reported in this paper.

Acknowledgements

This study was supported by the French National Research Foundation (ANR-16-CE05-0012-03). The authors gratefully acknowledge HotBlock OnBord (HBOB) for supplying the materials and the Deutsches Elektronen-Synchrotron, Germany; DESY, Germany for provision beamtime on P07.

References

[1] D. Champier, Thermoelectric generators: a review of applications, Energy Convers. Manag. 140 (2017) 167–181, https://doi.org/10.1016/j.enconman.2017.02.070.
[2] K. Koumoto, T. Mori (Eds.), Thermoelectric Nanomaterials: Materials Design and Applications, Springer-Verlag, Berlin Heidelberg, 2013. https://www.springer.com/gp/book/9783642375361. (Accessed 9 October 2019).
[3] Y. Gelbstein, J. Davidow, E. Leshem, O. Pinshow, S. Moisa, Significant lattice thermal conductivity reduction following phase separation of the highly efficient $Ge_xPb_{1-x}Te$ thermoelectric alloys, Phys. Status Solidi 251 (2014) 1431–1437, https://doi.org/10.1002/pssb.201451088.
[4] Y. Gelbstein, $Pb_{1-x}Sn_xTe$ alloys: Application considerations, J. Electron. Mater. 40 (2011) 533–536, https://doi.org/10.1007/s11664-010-1435-6.
[5] V.K. Zaitsev, M.I. Fedorov, E.A. Gurieva, I.S. Eremin, P.P. Konstantinov, A.Yu Samunin, M.V. Vedernikov, Highly effective Mg 2 Si 1 − x Sn x thermoelectrics, Phys. Rev. B 74 (2006), 045207, https://doi.org/10.1103/PhysRevB.74.045207.
[6] M.S. Ei-Genk, H.H. Saber, J. Sakamoto, T. Caillat, Life tests of a skutterudites thermoelectric unicouple (MAR-03), in: Proceedings ICT'03. 22nd International Conference on Thermoelectrics (IEEE Cat. No.03TH8726), IEEE, La Grande Motte, France, 2003, pp. 417–420, https://doi.org/10.1109/ICT.2003.1287537.
[7] N. Farahi, S. Prabhudev, G.A. Botton, J.R. Salvador, H. Kleinke, Nano- and microstructure engineering: an effective method for creating high efficiency magnesium silicide based thermoelectrics, ACS Appl. Mater. Interfaces 8 (2016) 34431–34437, https://doi.org/10.1021/acsami.6b12297.
[8] M. Mejri, Y. Thimont, B. Malard, C. Estournès, Characterization of the thermomechanical properties of p-type (MnSi1.77) and n-type (Mg2Si0.6Sn0.4) thermoelectric materials, Scripta Mater. 172 (2019) 28–32, https://doi.org/10.1016/j.scriptamat.2019.06.037.
[9] D.M. Rowe, Thermoelectrics Handbook : Macro to Nano, CRC Press, 2018, https://doi.org/10.1201/9781420038903.
[10] G. Skomedal, A. Burkov, A. Samunin, R. Haugsrud, H. Middleton, High temperature oxidation of Mg2(Si-Sn), Corrosion Sci. 111 (2016) 325–333, https://doi.org/10.1016/j.corsci.2016.05.016.
[11] D. Stathokostopoulos, D. Chaliampalias, E. Pavlidou, K.M. Paraskevopoulos, K. Chrissafis, G. Vourlias, Oxidation resistance of magnesium silicide under high-temperature air exposure, J. Therm. Anal. Calorim. 121 (2015) 169–175, https://doi.org/10.1007/s10973-015-4664-3.
[12] G. Skomedal, L. Holmgren, H. Middleton, I.S. Eremin, G.N. Isachenko, M. Jaegle, K. Tarantik, N. Vlachos, M. Manoli, T. Kyratsi, D. Berthebaud, N.Y. Dao Truong, F. Gascoin, Design, assembly and characterization of silicide-based thermoelectric modules, Energy Convers. Manag. 110 (2016) 13–21, https://doi.org/10.1016/j.enconman.2015.11.068.
[13] S. Yi, V. Attari, M. Jeong, J. Jian, S. Xue, H. Wang, R. Arroyave, C. Yu, Strain-induced suppression of the miscibility gap in nanostructured Mg2Si–Mg2Sn solid solutions, J. Mater. Chem. A. 6 (2018) 17559–17570, https://doi.org/10.1039/C8TA05798B.
[14] K. Yin, Q. Zhang, Y. Zheng, X. Su, X. Tang, C. Uher, Thermal stability of Mg2Si0.3Sn0.7 under different heat treatment conditions, J. Mater. Chem. C. 3 (2015) 10381–10387, https://doi.org/10.1039/C5TC01434D.
[15] M. Søndergaard, M. Christensen, K.A. Borup, H. Yin, B.B. Iversen, Thermal stability and thermoelectric properties of Mg2Si0.4Sn0.6 and Mg2Si0.6Sn0.4, J. Mater. Sci. 48 (2013) 2002–2008, https://doi.org/10.1007/s10853-012-6967-0.
[16] L. Zhang, X. Chen, Y. Tang, L. Shi, G.J. Snyder, J.B. Goodenough, J. Zhou, Thermal stability of $Mg_2Si_{0.4}Sn_{0.6}$ in inert gases and atomic-layer-deposited Al_2O_3 thin film as a protective coating, J. Mater. Chem. 4 (2016) 17726–17731, https://doi.org/10.1039/C6TA07611D.
[17] A. Sizov, H. Reardon, B.B. Iversen, P. Erhart, A.E.C. Palmqvist, Influence of phase separation and spinodal decomposition on microstructure of Mg2Si1−xSnx alloys, Cryst. Growth Des. 19 (2019) 4927–4933, https://doi.org/10.1021/acs.cgd.9b00013.
[18] M. Yasseri, A. Sankhla, H. Kamila, R. Orenstein, D.Y.N. Truong, N. Farahi, J. de Boor, E. Mueller, Solid solution formation in Mg2(Si,Sn) and shape of the miscibility gap, Acta Mater. 185 (2020) 80–88, https://doi.org/10.1016/j.actamat.2019.11.054.
[19] Sh Muntyanu, E.B. Sokolov, E.S. Makarov, Study of the Mg2Sn – Mg2Si system, J. Inorg. Mater. 2 (1966) 870–875.
[20] E.N. Nikitin, E.N. Tkalenko, V.K. Zaitsev, A.I. Zaslavskii, A.K. Kuznetsov, Study of phase diagram and some properties of solid solutions in the Mg2Si-Mg2Sn system, Izv. Akad. Nauk. SSSR - Neorganicheskiye Mater. 4 (1968) 1902–1906.
[21] Q. Zhang, T.J. Zhu, A.J. Zhou, H. Yin, X.B. Zhao, Preparation and thermoelectric properties of Mg2Si1-xSnx, Phys. Scripta T129 (2007) 123–126, https://doi.org/10.1088/0031-8949/2007/T129/028.
[22] I.-H. Jung, D.-H. Kang, W.-J. Park, N.J. Kim, S. Ahn, Thermodynamic modeling of the Mg–Si–Sn system, Calphad 31 (2007) 192–200, https://doi.org/10.1016/j.calphad.2006.12.003.
[23] A. Kozlov, J. Gröbner, R. Schmid-Fetzer, Phase formation in Mg–Sn–Si and Mg–Sn–Si–Ca alloys, J. Alloys Compd. 509 (2011) 3326–3337, https://doi.org/10.1016/j.jallcom.2010.12.052.
[24] R. Viennois, C. Colinet, P. Jund, J.-C. Tédenac, Phase stability of ternary anti-fluorite type compounds in the quasi-binary systems Mg2X–Mg2Y (X, Y = Si, Ge, Sn) via ab-initio calculations, Intermetallics 31 (2012) 145–151, https://doi.org/10.1016/j.intermet.2012.06.016.
[25] K. Romanjek, S. Vesin, L. Aixala, T. Baffie, G. Bernard-Granger, J. Dufourcq, High-performance silicon–germanium-based thermoelectric modules for gas exhaust energy scavenging, J. Electron. Mater. 44 (2015) 2192–2202, https://doi.org/10.1007/s11664-015-3761-1.
[26] J.B. Berkowitz-Mattuck, M. Rossetti, D.W. Lee, Enhanced oxidation of molybdenum disilicide under tensile stress: relation to pest mechanisms, Metall. Mater. Trans. B 1 (1970) 479–483, https://doi.org/10.1007/BF02811558.
[27] E. Fitzer, Plansee Proc, 2nd Seminar, 1955. Reutte/Tyrol.
[28] P. Qiu, X. Xia, X. Huang, M. Gu, Y. Qiu, L. Chen, "Pesting"-like oxidation phenomenon of p-type filled skutterudite Ce0.9Fe3CoSb12, J. Alloys Compd. 612 (2014) 365–371, https://doi.org/10.1016/j.jallcom.2014.05.215.
[29] A.D. Smigelskas, E.O. Kirkendall, Zinc Diffusion in Alpha Brass, The American Institute of Mining, Metallurgical, and Petroleum Engineers, 1946.
[30] B. Pieraggi, 2 - diffusion and solid state reactions, in: W. Gao, Z. Li (Eds.), Developments in High Temperature Corrosion and Protection of Materials, Woodhead Publishing, 2008, pp. 9–35, https://doi.org/10.1533/9781845694258.1.9.
[31] R.E. Smallman, A.H.W. Ngan, Chapter 7 - diffusion, in: R.E. Smallman, A.H.W. Ngan (Eds.), Modern Physical Metallurgy (Eighth Edition), Butterworth-Heinemann, Oxford, 2014, pp. 287–316, https://doi.org/10.1016/B978-0-08-098204-5.00007-9.
[32] H.M. Rietveld, A profile refinement method for nuclear and magnetic structures, J. Appl. Crystallogr. 2 (1969) 65–71, https://doi.org/10.1107/S0021889869006558.
[33] J. Rodríguez-Carvajal, Recent advances in magnetic structure determination by neutron powder diffraction, Phys. B Condens. Matter 192 (1993) 55–69, https://doi.org/10.1016/0921-4526(93)90108-I.